


# Optimization of extreme ultraviolet vortex beam based on high harmonic generation

Bo Xiao(肖礴), Yi-Wen Zhao(赵逸文), Fang-Jing Cheng(程方晶), Ge-Wen Wang(王革文), Wei Jiang(姜威), Yi-Chen Wang(王一琛), Jie Hu(胡杰), Hong-Jing Liang(梁红静), and Ri Ma(马日)

**Citation:**Chin. Phys. B, 2024, 33 (**5**): 054209. DOI: 10.1088/1674-1056/ad2bf0
Journal homepage: http://cpb.iphy.ac.cn; http://iopscience.iop.org/cpb

**What follows is a list of articles you may be interested in**

---

## Time-dependent variational approach to solve multi-dimensional time-dependent Schrödinger equation

Mingrui He(何明睿), Zhe Wang(王哲), Lufeng Yao(姚陆锋), and Yang Li(李洋)
Chin. Phys. B, 2023, 32 (**12**): 124206. DOI: 10.1088/1674-1056/acef03

## Role of quantum paths in generation of attosecond pulses

M R Sami and A Shahbaz†
Chin. Phys. B, 2020, 29 (**10**): 104207. DOI: 10.1088/1674-1056/ab9deb

## Atomic even-harmonic generation due to symmetry-breaking effects induced by spatially inhomogeneous field

Yue Guo(郭月), Aihua Liu(刘爱华), Jun Wang(王俊), Xueshen Liu(刘学深)
Chin. Phys. B, 2019, 28 (**9**): 094212. DOI: 10.1088/1674-1056/ab37fa

## Influence of intraband motion on the interband excitation and high harmonic generation

Rui-Xin Zuo(左瑞欣), Xiao-Hong Song(宋晓红), Xi-Wang Liu(刘希望), Shi-Dong Yang(杨士栋), Wei-Feng Yang(杨玮枫)
Chin. Phys. B, 2019, 28 (**9**): 094208. DOI: 10.1088/1674-1056/ab3446

## Femtosecond enhancement cavity with kilowatt average power

Jin Zhang(张津), Lin-Qiang Hua(华林强), Shao-Gang Yu(余少刚), Zhong Chen(陈忠), Xiao-Jun Liu(柳晓军)
Chin. Phys. B, 2019, 28 (**4**): 044206. DOI: 10.1088/1674-1056/28/4/044206

---

# Optimization of extreme ultraviolet vortex beam based on high harmonic generation

Bo Xiao(肖礴)[1], Yi-Wen Zhao(赵逸文)[1], Fang-Jing Cheng(程方晶)[1], Ge-Wen Wang(王革文)[1], Wei Jiang(姜威)[1], Yi-Chen Wang(王一琛)[1], Jie Hu(胡杰)[1], Hong-Jing Liang(梁红静)[2,†], and Ri Ma(马日)[1,‡]

[1] *Institute of Atomic and Molecular Physics, Jilin University, Changchun* 130012, *China*
[2] *College of Science, Jilin Institute of Chemical Technology, Jilin* 132022, *China*

(Received 8 December 2023; revised manuscript received 3 February 2024; accepted manuscript online 22 February 2024)

In high harmonic generation (HHG), Laguerre–Gaussian (LG) beams are used to generate extreme ultraviolet (XUV) vortices with well-defined orbital angular momentum (OAM), which have potential applications in fields such as microscopy and spectroscopy. An experimental study on the HHG driven by vortex and Gaussian beams is conducted in this work. It is found that the intensity of vortex harmonics is positively correlated with the laser energy and gas pressure. The structure and intensity distribution of the vortex harmonics exhibit significant dependence on the relative position between the gas jet and the laser focus. The ring-like structures observed in the vortex harmonics, and the interference of quantum paths provide an explanation for the distinct structural characteristics. Moreover, by adjusting the relative position between the jet and laser focus, it is possible to discern the contributions from different quantum paths. The optimization of the HH vortex field is applicable to the XUV, which opens up a new way for exploiting the potential in optical spin or manipulating electrons by using the photon with tunable orbital angular momentum.

**Keywords:** high harmonic generation, phase matching, extreme ultraviolet vortex beam, quantum path interference

**PACS:** 42.65.Ky, 42.65.Re, 47.32.cb **DOI:** 10.1088/1674-1056/ad2bf0

## 1. Introduction

Vortex beams are well known for their helical phase structure,[1] represented by the electric field equation $\boldsymbol{E}(r,\varphi,z) = E_0(r,\varphi,z)\exp(\mathrm{i}l\varphi)\exp(-\mathrm{i}kz)$ where $E_0(r,\varphi,z)$ is the amplitude of the vortex driving field at position $z$, $\exp(\mathrm{i}l\varphi)$ describes the spiral phase factor of the vortex beam, $\varphi$ denotes the azimuthal angle, $l$ represents the topological charge of the vortex beam and indicates the wave number.[2] In 1992, Allen *et al.* found that a Laguerre–Gaussian (LG) vortex beam carries an orbital angular momentum (OAM) of $l\hbar$ per photon.[3] The phase singularity of the vortex beam center is caused by the phase uncertainty of the beam, which determines the unique doughnut shape intensity distribution of the vortex beam. Generally, vortex beams can be LG beams,[3] Hermite–Gaussian (HG) beams,[4] or Bessel–Gauss (BG) beams.[5] During the past decades, vortex beams were extended to almost every field of advanced optics such as optical manipulation,[6] quantum information processing,[7] optical communication,[8] chiral molecules recognition,[9] or the interaction between atoms and molecules in order to observe angular momentum transfer process.[10] Vortex beams can be generated through mode converters,[11] computer-generating holograms,[12] spiral phase plates,[13] and spatial light modulators.[14]

It is crucial to obtain vortex beams in extreme ultraviolet (XUV) region if one wishes to enforce the OAM of the vortex field involvement in electron motion within an atom or molecule. In recent years, the high harmonic generation (HHG) process induced by a vortex IR beam interacting with a gas medium has enabled the generation of XUV vortex beams.[15,16] Unlike synchrotron light sources and free-electron-laser (FEL), the HHG process offers the advantage of being conducted on a tabletop scale, making it a powerful tool for generating XUV light source or an attosecond pulse.[17–19] Due to the emitted high harmonics containing information about the interaction and electronic dynamics, HHG has been introduced into different systems, including gases,[20] plasmas,[21] and solids.[22–26] The HHG process has also been studied extensively in theory and experiment for generating XUV vortices, which has emerged as an important research area.[27–33] Researchers have made significant progress in understanding and manipulating XUV vortex beams generated through the HHG process. Zürch *et al.* experimentally found that the phase singularity of vortex properties of the driving beam can be transferred into the HHG.[28] Subsequent experimental and theoretical studies have established the unambiguous relationship between the topological charge of the driving beam and the harmonic order, *i.e.*, the topological charge $l_q$ equal to $q \times l$ where $q$ represents the harmonic order and $l$ is the topological charge of the driving beam.[16,34] Various methods have been employed to tune and control the topological charge of XUV vortex beams by using specific driving laser configurations, such as perturbation

†Corresponding author. E-mail: lianghongjing@jlict.edu.cn
‡Corresponding author. E-mail: rma@jlu.edu.cn

© 2024 Chinese Physical Society and IOP Publishing Ltd 

techniques and two-color driving laser beams.[35–37] Recently, it has been increasingly recognized that the phase matching and quantum trajectory contribution of vortex HHG are crucial for the intensity and spatial structure of the generated high harmonics. For example, Hernández *et al.* theoretically simulated the spatial superposition of different quantum trajectories of vortex harmonics by means of an improved strong-field approximation model.[31] Paufler *et al.* theoretically simulated phase matching of different OAMs on both one- and two-dimensional scales, respectively.[38] Jin *et al*. theoretically investigated the phase-matching mechanism by using nonzero OAM vortex beams through the HHG process and demonstrated that the coherence length and phase distribution of the vortex harmonics strongly depend on the relative position of the gas target with respect to the laser focus.[39] In a follow-up study from the same group, they investigated the generation of an XUV vortex beam by mixing two different topological LG beams as the driving beam. The results revealed that the phase matching of HHG vortices depends on the position of the gas medium and the contribution of short or long trajectories.[40] Gao *et al.* experimentally characterized the contribution of different quantum trajectories by measuring the diameters of vortex harmonics at different laser focus positions.[33]

In this work, we aim to experimentally investigate and compare the generation of the vortex and Gaussian XUV beams through the HHG process. We measure the dependence of the intensity of harmonics on both laser energy and gas pressures. Additionally, by varying the relative position of the gas jet to the laser focus, we also focus on investigating the characteristics of the intensity and pattern of the vortex harmonics. This study indicates that the understanding of phase-matching mechanisms and interference of quantum paths in HHG is significantly important for generating and optimizing XUV vortex beams.

## 2. Experiments

Generating and detecting gas HHG induced by strong laser fields is performed on a home-built spectrometer as shown in Fig. 1. The combination of a half-wave plate and a Glan-laser polarizer is used to regulate the laser energy. To generate vortex driving beam, the pulse output from a Ti:sapphire laser system (1 kHz, 35 fs, 800 nm) is directed to a beam expander to convert the Gaussian wavefront into an approximate plane wavefront. The diameter of the plane wavefront beam is 10 mm, which is adjusted with an iris. Subsequently, the plane wavefront beam is structured by a topological charge with $l = 1$ of the spiral phase plate (RPC, VPP-1b), to obtain the driving vortex beam with a transversal spiral-phase structure around the beam axis. Then the vortex beam is focused on a 100-μm diameter nozzle orifice through a convex lens ($f = 300$ mm) to produce high harmonics. The generated harmonics are reflected by a gold-coated mirror and diffracted by a spherical grating with a groove density of 1200 grooves/mm. An aluminum foil is placed in front of the slit to filter the fundamental frequency laser. The slit is used to improve the resolution of harmonic spectra. And the harmonic spectra are detected by a micro-channel plate (MCP) and phosphor screen. The HHG images are recorded by a charge-couple device camera (Hamamatsu ORCA R2).

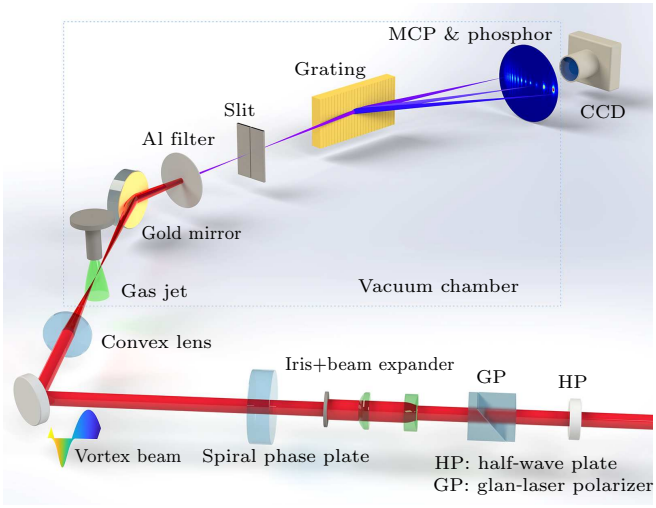



**Fig. 1.** Schematic diagram of experimental setup for harmonic generation from Ar interaction with vortex beam.

## 3. Results and discussion

In this study, the measured harmonic spectra of Ar driven with Gaussian beams and vortex beams are shown in Figs. 2(a) and 2(c), respectively, while the corresponding integrated HHG intensities are shown in Figs. 2(b) and 2(d). Comparing Fig. 2(c) with Fig. 2(a), clear split structure of each order harmonic driven by the vortex beam is observed. The dark missing part (red dotted line in Fig. 2(c)) is corresponding with the phase singularity of the vortex beam, which is caused by the vortex properties being imprinted from the IR driving beam to the generated XUV beam.[16] And the singularity is the further proof of XUV vortex based on HHG.

To further explore the characteristics of vortex harmonics, we compare and investigate the laser energy dependence on two types of HHGs. Figure 3 shows the dependence of harmonic intensity of H21–H31 on laser energy driven by Gaussian beam (Fig. 3(a)) and vortex beam (Fig. 3(b)) (the notation H$n$ refers to the $n$-th-order HHG). As shown in the figures, the H$n$ intensity peaks are located at approximately 1.6 mJ and 0.7 mJ for the Gaussian driving beam and the vortex driving beam, respectively, which indicates that the harmonic intensity has reached a saturation point under the experimental conditions. It is worth noticing that the harmonics generated by the Gaussian beam are slightly stronger than those generated by the vortex beam when the harmonic intensity reaches a maximum. This difference caused by a different phase-matching mechanism for the two different driving beam cases, which will be discussed in detail in the following sections.

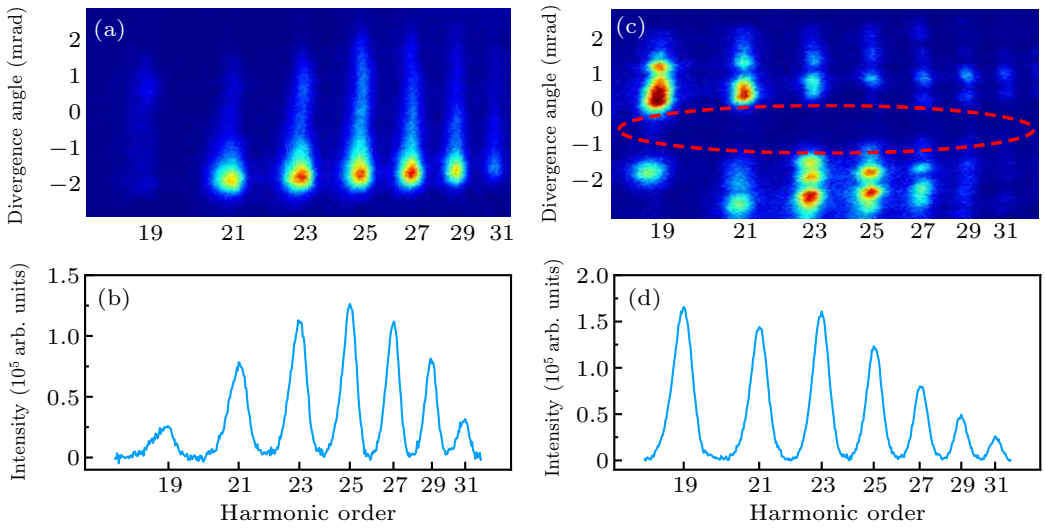



**Fig. 2.** Part of HHG spectra of Ar irradiated by an 800 nm, 35 fs linearly polarized (a) Gaussian and (c) vortex driving laser field, with red dotted line denoting the location of the singularity and ((b) and (d)) their corresponding integrated HHG intensity.

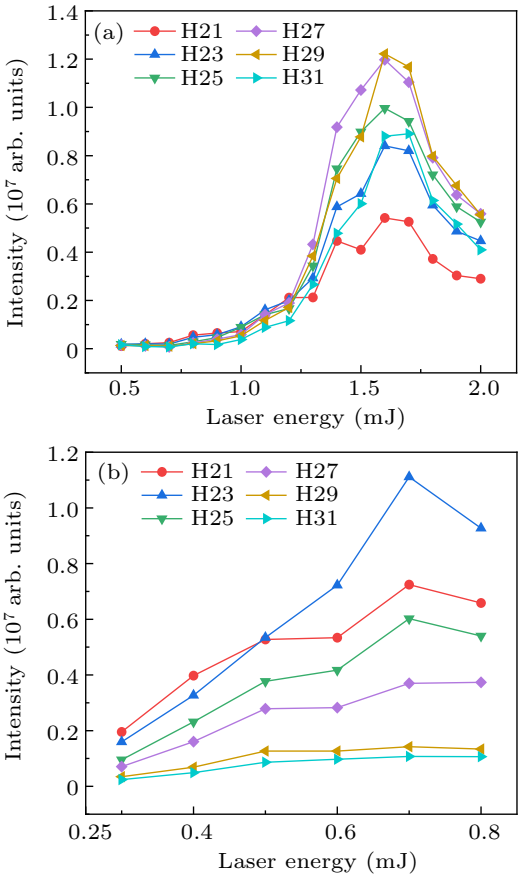



**Fig. 3.** Measured harmonic intensities of H21 (red circles), H23 (blue triangles), H25 (green inverted triangles), H27 (purple diamonds), H29 (yellow left triangle), and H31 (cyan right triangle) as a function of the laser energy. The harmonic driven by (a) Gaussian beam when pressure of gas jet at 3 atm (1 atm = $1.01325\times10^5$ Pa) and (b) vortex beam when pressure of gas jet at 2.6 atm, respectively.

The dependence of harmonic intensity on gas pressure is shown in Fig. 4. Figure 4(a) shows that the harmonics intensity produced by the Gaussian beam grows monotonically with gas pressure increasing. For the harmonics from the vortex beam, the intensities rise to a slight maximum point at 2.6 atm and continues to increase as shown in Fig. 4(b).

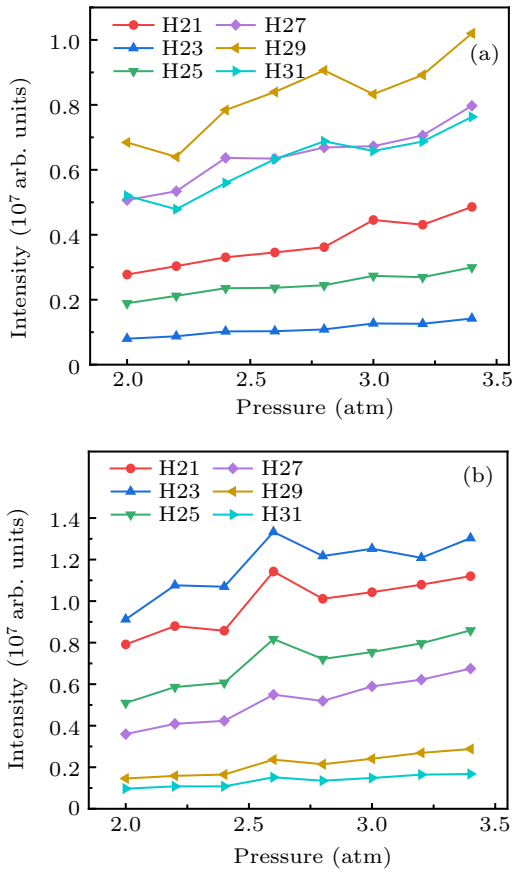



**Fig. 4.** Measured (a) Gaussian harmonic intensity and (b) vortex harmonic intensity *versus* gas pressure with laser energy of 1.6 mJ and 0.7 mJ, respectively.

The achieving of HHG with high conversion efficiency requires both the microscopic and macroscopic properties of the process to be optimized. The microscopic response is well described by the semi-classical three-step model.[41] Macroscopically, the phase-matching is essential for the HHG output emission. The phase matching mechanism is mainly influ-

enced by the phase gradient of the driving beam, the plasma dispersion, the neutral gas dispersion, and the atomic dipole phase.[20,42] The degree of phase mismatch is given as $\Delta k = \Delta k_{\rm g} + \Delta k_{\rm n} + \Delta k_{\rm p} + \Delta k_{\rm d}$, where $\Delta k_{\rm g}$ denotes the driving beam phase gradient, $\Delta k_{\rm n}$ is the neutral gas dispersion, $\Delta k_{\rm p}$ is the plasma dispersion, and $\Delta k_{\rm d}$ is the atomic dipole phase. Previous studies have shown that the Gaussian driving beam phase gradient $\Delta k_{\rm g}$ and the atomic dipole phase $\Delta k_{\rm d}$ play a major role in the harmonic phase matching under the 300-mm tight focus conditions.[43] Meanwhile, the atomic dipole phase of the emitted radiation depends on the local intensity and different atoms are exposed to different local intensities of a vortex beam. It is necessary to introduce a supernumerary focal phase term $\Delta k_{\rm f}$ due to the zero intensity at the vortex beam axis.[38] All the contributions to the phase mismatch will be discussed later.

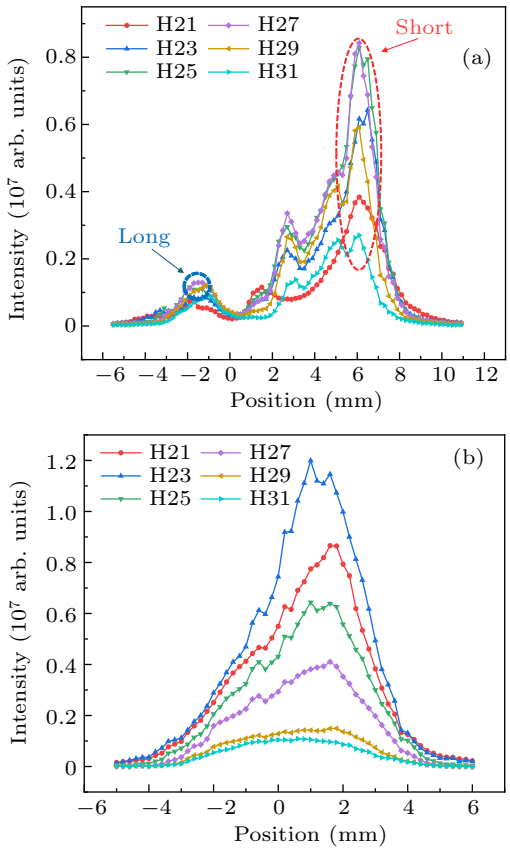



**Fig. 5.** Measured different order harmonics' intensities of Ar as a function of the position of the gas jet relative to the laser focus, the driving laser field with laser energy of 1.6 mJ and 0.7 mJ, gas jet pressure of 3 atm and 2.6 atm respectively for (a) Gaussian beam and (b) vortex beam.

To assess the harmonic intensity distributions at different positions relative to the laser focus and jet, the intensity dependent Gaussian and vortex harmonics are measured as shown in Figs. 5(a) and 5(b), respectively. There are mainly two electron quantum trajectories contributing to the harmonic emission, which are referred to as short trajectory and long trajectory according to their excursion time.[43–46] The short trajectory is more likely to achieve collinear phase-matching on the axis of propagation at the gas jet behind the laser focus. However, the noncollinear phase-matching where the gas jet in front of the laser focus for long trajectory is off axis.[47] As shown in Fig. 5(a), two maximum phase dependent electronic trajectories elucidated by Gaarde *et al.*[46] are clearly observed in the harmonic spectra at the positions of −1.5 mm and 5.5 mm, *i.e.*, the gas jet is placed at 1.5 mm in front of and 5.5 mm behind the laser focus respectively (see dashed circles labeled in Fig. 5(a)). These two positions are in accordance with the presence of classic long trajectory and short trajectory in harmonic spectra. While vortex harmonics are not separated by the two quantum paths, reaching only a maximum value at the position near 1.4 mm as indicated in Fig. 5(b).

Our experimental results as shown in Fig. 5 indicate that the distribution of harmonics strongly depends on the relative positions of the laser focus and the gas jet, which is consistent with the theoretical predictions by Jin *et al.*[39]

To further elucidate this observation, we investigate the structure distributions of vortex harmonics as shown in Fig. 6. Theoretically, Hernández *et al.* have analyzed that the generation and propagation effects of the XUV vortex beam and reported the intensity distribution of the vortex harmonic beam that has a ring-like structure.[16] In Fig. 6(a), the red dotted line represents the original circular distribution of the vortex harmonics and the central dark part of the circle is phase singularity. However, the distribution of spectrogram in Fig. 6(a) becomes a double-fringe profile in shape by a slit. For the sake of understanding, we only show the structure distributions of the upper half of H23 vortex harmonics in Figs. 6(b)–6(d), for the laser focus located at −1.4 mm, 0 mm, and 1.4 mm relative to the gas jet, respectively. The left panels in Figs. 6(b)–6(d) are the integrated intensities in the corresponding vertical directions. Based on the semi-classical picture, the contributions from different electron trajectories will interfere.[48] Apparently, the interference between short trajectory and long trajectory plays a significant role in generating vortex harmonics. For H23, the spot splitting caused by short-trajectory electrons can be clearly observed where the gas jet is 1.4 mm in front of or at the laser focus in Figs. 6(b) and 6(c). In contrast, the gas jet is 1.4 mm behind the laser focus, contributing to the weakening or disappearing of the two emission branches because the interference becomes significant in Fig. 6(d).

Figure 7 shows the integrated harmonic intensities generated at three different relative positions between the laser focus and the gas jet. The most notable feature is that the most efficient generation of all the orders of vortex HHG is achieved when the gas jet is located at 1.4 mm behind the laser focus. Now we return to the discussion of phase-matching for the optimized intensity of vortex harmonic. As mentioned before,

the neutral gas dispersion causes a positive phase mismatch, whereas plasma dispersion triggers off a negative phase mismatch, with their magnitudes balancing each other based on the gas pressure.[43,49] The contribution from the driving beam phase gradient is positive and the focal phase has a constant negative value, and thus counteracts the increasing contribution of a part of beam phase gradient.[38] For the total phase-matching, the contribution of the atomic dipole phase is positive if the gas jet appears in front of the laser focus, whereas it is negative if the gas jet is behind the laser focus.[38] This explains why the harmonic intensity of the gas jet behind laser focus is greater than that in front of the laser focus, which is consistent with theoretical results.[39] Furthermore, we note that the harmonic yields in the cut-off region (H29 and H31) remain relatively constant regardless of changes at the focal position, which is attributed to the presence of a single quantum trajectory contribution factor.[50,51] The summarizing of the experimental observations indicate that there are striking changes in the intensity and structure of the vortex harmonics when the gas target position with respect to the driving laser focus is changed, which is in agreement with the theoretical prediction in Ref. [39].

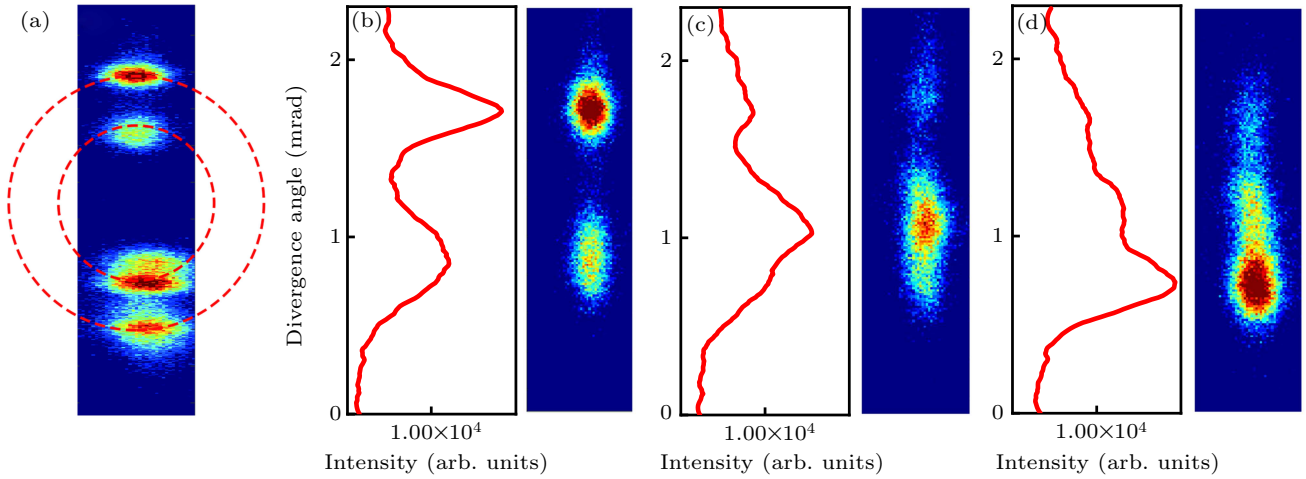



**Fig. 6.** Distribution of (a) total and ((b)–(d)) upper half of H23 vortex harmonic intensity with the center of the gas jet placed at (b) 1.4 mm in front of, (c) at laser focus, and (d) 1.4 mm behind the laser focus, respectively, with red dashed circle showing H23 vortex harmonic initial intensity distribution in panel (a). Left of the panels (b)–(d): the intensity of integration in the corresponding vertical direction.

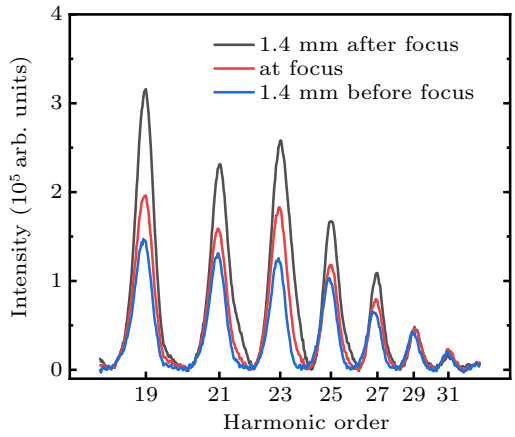



**Fig. 7.** Integrated vortex harmonic spectra obtained at three different positions of gas jet relative to laser focus.

## 4. Conclusions

Our study provides valuable insights into the phase matching of vortex high-harmonic generation (HHG) and presents a versatile approach to optimizing extreme ultraviolet (XUV) vortex beams. The results reveal significant dependence of the structure and intensity distribution of the vortex harmonics on the relative position between the gas jet and the laser focus. Specifically, when the gas jet is located in front of or at the focus, the radiation from single quantum path leads to the formation of multi-ringed pattern vortex harmonics structures. Conversely, when the gas jet is located behind the laser focus, the combination of short quantum path and long quantum path contributes to the weakening of multi-ringed structure. It is possible to discern the contributions among different quantum paths by adjusting the relative position between the gas jet and the laser focus. The HHG with LG beams has potential applications in many fields such as microscopy and spectroscopy including the creation of circularly polarized XUV vortices with well-defined orbital angular momentum (OAM). These vortices can be used for imaging and manipulating nanoscale structures, as well as for studying the electronic and magnetic properties of materials. Additionally, the HHG vortices also allow for the investigation of ultrafast dynamics in atoms and molecules, which has implications for fields such as chemistry and materials science.

## Acknowledgements

Project supported by the National Natural Science Foundation of China (Grant Nos. 11974137, 92250306, and 12304302), the National Key Program for Science and Technology Research and Development (Grant No. 2019YFA0307700), the Natural Science Foundation of Jilin Province, China (Grant Nos. YDZJ202101ZYTS157 and

YDZJ202201ZYTS314), and the Scientific Research Foundation of Jilin Provincial Education Department, China (Grant No. JJKH20230283KJ).

## References


[1] Yao A M and Padgett M J 2011 *Adv. Opt. Photon.* **3** 161
[2] Shen Y, Wang X, Xie Z, Min C, Fu X, Liu Q, Gong M and Yuan X 2019 *Light Sci. Appl.* **8** 90
[3] Allen L, Beijersbergen M W, Spreeuw R J and Woerdman J P 1992 *Phys. Rev. A* **45** 8185
[4] Laabs H, Gao C and Weber H 1999 *J. Mod. Opt.* **46** 709
[5] Bagini V, Frezza F, Santarsiero M, Schettini G and Spagnolo G S 1996 *J. Mod. Opt.* **43** 1155
[6] Grier D G 2003 *Nature* **424** 810
[7] Wang J, Yang J Y, Fazal I M, Ahmed N, Yan Y, Huang H, Ren Y, Yue Y, Dolinar S, Tur M and Willner A E 2012 *Nat. Photon.* **6** 488
[8] Willner A E, Huang H, Yan Y, Ren Y, Ahmed N, Xie G, Bao C, Li L, Cao Y, Zhao Z, Wang J, Lavery M P J, Tur M, Ramachandran S, Molisch A F, Ashrafi N and Ashrafi S 2015 *Adv. Opt. Photon.* **7** 66
[9] Forbes K A 2019 *Phys. Rev. Lett.* **122** 103201
[10] De Ninno G, Wtzel J, Ribič P R, *et al.* 2020 *Nat. Photon.* **14** 554
[11] Tamm C and Weiss C 1990 *J. Opt. Soc. Am. B* **7** 1034
[12] Heckenberg N, McDuff R, Smith C and White A 1992 *Opt. Lett.* **17** 221
[13] Turnbull G A, Robertson D, Smith G, Allen L and Padgett M 1996 *Opt. Commun.* **127** 183
[14] Forbes A, Dudley A and McLaren M 2016 *Adv. Opt. Photon.* **8** 200
[15] Géneaux R, Camper A, Auguste T, Gobert O, Caillat J, Taieb R and Ruchon T 2016 *Nat. Commun.* **7** 12583
[16] Hernandez-Garcia C, Picon A, San Roman J and Plaja L 2013 *Phys. Rev. Lett.* **111** 083602
[17] Xin M, Safak K, Peng M Y, Kalaydzhyan A, Wang W T, Mucke O D, and Kartner F X 2017 *Light Sci. Appl.* **6** e16187
[18] Paul P M, Toma E S, Breger P, Mullot G, Augé F, Balcou P, Muller H G and Agostini P 2001 *Science* **292** 1689
[19] Bostedt C, Bozek J, Bucksbaum P, Coffee R, Hastings J, Huang Z, Lee R, Schorb S, Corlett J and Denes P 2013 *J. Phys. B: At. Mol. Opt. Phys.* **46** 164003
[20] Winterfeldt C, Spielmann C and Gerber G 2008 *Rev. Mod. Phys.* **80** 117
[21] Teubner U and Gibbon P 2009 *Rev. Mod. Phys.* **81** 445
[22] Lang Y, Peng Z Y and Zhao Z X 2022 *Chin. Phys. Lett.* **39** 114201
[23] Peng Z Y, Lang Y, Zhu Y L, Zhao J, Zhang D W, Zhao Z X and Yuan J M 2023 *Chin. Phys. Lett.* **40** 054203
[24] Zhang C P and Miao X Y 2023 *Chin. Phys. Lett.* **40** 124201
[25] Qiao Y, Chen J Q, Zhou S S, Chen J G, Jiang S C and Yang Y J 2024 *Chin. Phys. Lett.* **41** 014205
[26] Ghimire S and Reis D A 2018 *Nat. Phys.* **15** 10
[27] Popmintchev T, Chen M-C, Arpin P, Murnane M M and Kapteyn H C 2010 *Nat. Photon.* **4** 822
[28] Zürch M, Kern C, Hansinger P, Dreischuh A and Spielmann C 2012 *Nat. Phys.* **8** 743
[29] Patchkovskii S and Spanner M 2012 *Nat. Phys.* **8** 707
[30] Han J X, Guan Z, Wang B Y and Jin C 2023 *Chin. Phys. B* **32** 124210
[31] Hernández-García C, Román J S, Plaja L and Picón A 2015 *New. J. Phys.* **17** 093029
[32] Wang B Y, Han J X and Jin C 2023 *Chin. Phys. B* **32** 124208
[33] Gao J X, Yang C, Ge X C, Zheng Y H, Zeng Z N and Li R X 2023 *Opt. Express* **32** 871
[34] Gariepy G, Leach J, Kim K T, Hammond T J, Frumker E, Boyd R W and Corkum P B 2014 *Phys. Rev. Lett.* **113** 153901
[35] Gauthier D, Ribič P R, Adhikary G, Camper A, Chappuis C, Cucini R, DiMauro L F, Dovillaire G, Frassetto F, Géneaux R, Miotti P, Poletto L, Ressel B, Spezzani C, Stupar M, Ruchon T and De Ninno G 2017 *Nat. Commun.* **8** 14971
[36] Kong F Q, Zhang C M, Bouchard F, Li Z Y, Brown G G, Ko D H, Hammond T J, Arissian L, Boyd R W, Karimi E and Corkum P B 2017 *Nat. Commun.* **8** 14971
[37] Rego L, Roman J S, Picon A, Plaja L and Hernandez-Garcia C 2016 *Phys. Rev. Lett.* **117** 163202
[38] Paufler W, Böning B and Fritzsche S 2019 *Phys. Rev. A* **100** 013422
[39] Jin C, Li B, Wang K, Xu C, Tang X, Yu C and Lin C D 2020 *Phys. Rev. A* **102** 033113
[40] Guan Z, Yin Z M and Jin C 2022 *Phys. Rev. A* **105** 023107
[41] Corkum P B 1993 *Phys. Rev. Lett.* **71** 1994
[42] Rudawski P, Heyl C, Brizuela F, Schwenke J, Persson A, Mansten E, Rakowski R, Rading L, Campi F and Kim B 2013 *Rev. Sci. Instrum.* **84** 073103
[43] Niu Y, Liu F Y, Liu Y, Liang H J, Yang Y J, Ma R and Ding D J 2017 *Opt. Commun.* **397** 118
[44] Balcou P, Salières P, L'Huillier A and Lewenstein M 1997 *Phys. Rev. A* **55** 3204
[45] Balcou P, Dederichs A S, Gaarde M B and L'Huillier A 1999 *J. Phys. B:. At. Mol. Opt. Phys.* **32** 2973
[46] Gaarde M B, Salin F, Constant E, Balcou P, Schafer K J, Kulander K C and L'Huillier A 1999 *Phys. Rev. A* **59** 1367
[47] Salières P, L'Huillier A and Lewenstein M 1995 *Phys. Rev. Lett.* **74** 3776
[48] Schapper F, Holler M, Auguste T, Zaïr A, Weger M, Salières P, Gallmann L and Keller U 2010 *Opt. Express* **18** 2987
[49] Wang G L, Jin C, Le A T and Lin C D 2011 *Phys. Rev. A* **84** 053404
[50] Lewenstein M, Salieres P and L'Huillier A 1995 *Phys. Rev. A* **52** 4747
[51] Gaarde M B and Schafer K J 2002 *Phys. Rev. A* **65** 031406